Applied Clay Science 129 (2016) 27–34

Contents lists available at ScienceDirect

Applied Clay Science

journal homepage: www.elsevier.com/locate/clay

Research paper

$BiVO_4$/Fe/Mt composite for visible-light-driven degradation of acid red 18

Tianyuan Xu [a,b,c], Runliang Zhu [a,b,*], Jianxi Zhu [a,b], Xiaoliang Liang [a,b], Yun Liu [d], Yin Xu [d], Hongping He [a,b]

[a] CAS Key Laboratory of Mineralogy and Metallogeny, Guangzhou Institute of Geochemistry, Chinese Academy of Sciences, 511 Kehua Street, Guangzhou 510640, China
[b] Guangdong Provincial Key Laboratory of Mineral Physics and Materials, 511 Kehua Street, Guangzhou 510640, China
[c] University of Chinese Academy of Sciences, 19 Yuquan Road, Beijing 100049, China
[d] Xiangtan University, Hunan, 411105, China

ARTICLE INFO

Article history:
Received 11 January 2016
Received in revised form 20 April 2016
Accepted 21 April 2016
Available online 5 May 2016

Keywords:
Visible light
Photocatalysis
Bismuth vanadate
Hydroxy-iron pillared montmorillonite
OH radicals

ABSTRACT

This work described a strategy for loading bismuth vanadate ($BiVO_4$) on hydroxy-iron pillared montmorillonite (Fe/Mt), in which vanadate and bismuth were successively loaded on Fe/Mt to synthesize a $BiVO_4$/Fe/Mt composite with high photo-Fenton catalytic activity. The structural characteristics of the resulting materials were studied using X-ray diffraction, inductively coupled plasma mass spectrometry, nitrogen adsorption–desorption isotherms, and UV–vis diffuse reflectance spectra. Then, the photo-Fenton catalytic activity of the obtained catalysts was tested using acid red 18 (AR18) as a model contaminant under visible light irradiation. Furthermore, the concentration of hydroxyl radical (•OH) was studied by high performance liquid chromatography. The results indicated that $BiVO_4$ loaded not only on the outer surface but also into the interlayers of Fe/Mt. The 8%$BiVO_4$/Fe/Mt composite exhibited high photocatalytic activity, and the decolorization efficiency, TOC removal efficiency of AR18, and the production of •OH by $BiVO_4$/Fe/Mt were higher than those by Fe/Mt. The high removal efficiency of AR18 and remarkable •OH generation performance by $BiVO_4$/Fe/Mt should be attributed to the presence of $BiVO_4$, which can accelerate the reduction of Fe^{3+} to Fe^{2+} by providing photo-induced electrons from $BiVO_4$. In addition, the leached amount of Fe from $BiVO_4$/Fe/Mt was 0.32 mg/L after 180 min reaction, much smaller than that from Fe/Mt (0.66 mg/L). The results of this work suggest that the introduction of semiconductor materials may be a feasible way for enhancing the photo-Fenton catalytic activity of heterogeneous photo-Fenton catalysts.

1. Introduction

Montmorillonite (Mt) has been found as a suitable catalyst support because of its low cost and unique structural characteristics such as a nano-sized layered structure and possession of exchangeable inorganic cations (Ramesh et al., 2007; Garrido-Ramírez et al., 2010). Intercalating Mt with various functional intercalants can always increase the basal spacing and specific surface area of Mt, and the reactive sites on Mt as well (Herney-Ramirez et al., 2010). As such, large amounts of Mt-based catalysts have been synthesized by intercalating Mt with various hydroxy-metals (Ai and Hameed, 2011), such as hydroxy-iron intercalated Mt (Fe/Mt) (Feng et al., 2003, 2004; Wu et al., 2009), hydroxy-aluminum intercalated Mt (Epstein and Yariv, 2003; Karamanis and Assimakopoulos, 2007), hydroxy-iron–aluminum intercalated Mt (Konstantinou et al., 2000; Carriazo et al., 2003), etc.

Thereunto, Fe/Mt can be used as a heterogeneous photo-Fenton catalyst for the degradation of organic contaminants in water, and large amounts of researches have shown that various organic contaminants can be degraded under UV light irradiation (Chen and Zhu, 2007; Daud et al., 2010; De León et al., 2013). As the UV light occupies only 4% of solar irradiance that reaches the surface of the earth (Kavitha et al., 2013) while artificial UV light sources generally consume large quantities of electrical power, the industrial application of Fe/Mt as a heterogeneous photo-Fenton catalyst has been limited. In recent years, several studies have examined the degradation of organic contaminants by Fe/Mt under visible light irradiation (Chen et al., 2009), but the catalytic efficiency is far lower than that under UV light irradiation. As such, developing new approaches to enhance the catalytic degradation efficiency of Fe/Mt under visible light irradiation is of high importance for its pollution control applications.

On the other hand, several studies showed that iron oxide can act as an electron-transfer channel and acceptor in iron oxide/semiconductor composites, which can then suppress the recombination of a photogenerated electron–hole (Wang et al., 2014). For instance, Xi et al. (2011) synthesized an Fe_3O_4/WO_3 core–shell visible light photocatalyst, in which the conductive Fe_3O_4 microspheres (the core)

* Corresponding author at: CAS Key Laboratory of Mineralogy and Metallogeny, Guangzhou Institute of Geochemistry, Chinese Academy of Sciences, 511 Kehua Street, Guangzhou 510640, China.
E-mail address: zhurl@gig.ac.cn (R. Zhu).

http://dx.doi.org/10.1016/j.clay.2016.04.018
0169-1317/

were used as charge collectors to transport the photogenerated charges from WO_3, leading to a significant enhancement of photodegradation activity toward rhodamine B (RhB). Ge et al. (2012) reported that the presence of Fe^{3+} can prevent the recombination of the electron–hole produced on $BiVO_4$, as Fe^{3+} could accept the photogenerated electrons, by which the catalytic degradation of RhB was evidently enhanced. Enlightened by these studies, we expect that the presence of semiconductors (e.g., $BiVO_4$) on Fe/Mt can accelerate the reduction of Fe^{3+} into Fe^{2+} by photoinduced electrons, which may then improve the photo-Fenton catalytic activity of Fe/Mt for the degradation of organic contaminants under visible light irradiation.

In the present work, Fe/Mt was synthesized and further used as a host material to load $BiVO_4$, with the purpose of synthesizing new material (i.e., $BiVO_4$/Fe/Mt) with high photo-Fenton catalytic activity under visible light irradiation. Toward this aim, vanadate (V) and bismuth (Bi) were successively loaded on Fe/Mt, and then the microstructure of the resulting $BiVO_4$/Fe/Mt and its photocatalytic activities in the decolorization and mineralization of acid red 18 (AR18) were studied. In addition, generation of OH radicals (•OH) and stability of photocatalysts in the heterogeneous photo-Fenton systems were further examined. The results of this work may provide novel information for enhancing the photo-Fenton catalytic activity of heterogeneous photo-Fenton catalysts.

2. Experimental sections

2.1. Materials

Sodium exchanged Mt from Anji County, China, with the cation exchange capacity (CEC) of 1.05 meq/g, and the chemical formula $Na_{0.19}Ca_{0.14}(Al_{1.47}Fe_{0.04}Mg_{0.49})Si_4O_{10}(OH)_2 \cdot nH_2O$ was used as the starting material (Wang et al., 2015). AR18 was purchased from the National Medicine Group Chemical Reagent Co., Ltd. (China) and used without further purification. Hydrogen peroxide (H_2O_2, 30 wt.%), sodium carbonate (Na_2CO_3), ferric nitrate ($Fe(NO_3)_3 \cdot 9H_2O$), bismuth nitrate ($Bi(NO_3)_3 \cdot 5H_2O$), ammonium metavanadate (NH_4VO_3), nitric acid (HNO_3), sodium hydroxide (NaOH), dimethyl sulfoxide (DMSO), and 2,4-dinitrophenylhydrazine (DNPH) were of analytical grade and obtained from the Guangzhou Chemical Reagent Factory (Guangzhou, China).

2.2. Catalyst preparation

The preparation process of $BiVO_4$/Fe/Mt was as follows. 0.2 mol/L Na_2CO_3 was slowly added to 0.2 mol/L $Fe(NO_3)_3$ solution under magnetic stirring at 60 °C until the molar ratio of OH^-/Fe^{3+} reached 1. Then, the solution was aged for 24 h. After that the hydroxy-iron solution was added to the 2 wt.% Mt dispersion under stirring for 24 h. The final Fe^{3+}/clay ratio was equal to 5 mmol/g of dry Mt. After stirring for 24 h at 60 °C, the product was centrifuged and washed. The resulting material was denoted as Fe/Mt.

After that, 8 g Fe/Mt was dispersed in 400 mL water again, which was then slowly mixed with 0.4×10^{-2} mol/L NH_4VO_3 solution under magnetic stirring until the molar ratio of V/Fe reached a desired value (0.01, 0.02, 0.04, 0.08, 0.1, or 0.15). After stirring for 24 h, the product was centrifuged and washed. The resulting material was denoted as V/Fe/Mt. In order to simulate the adsorption process, the preparation process of V/Fe/Mt was conducted at room temperature. Finally, a desired amount of $Bi(NO_3)_3 \cdot 5H_2O$ was added into deionized water to obtain 0.4×10^{-2} mol/L $Bi(NO_3)_3$ solution. To avoid the formation of Bi precipitation by hydrolysis, the water temperature was kept higher than 90 °C (Guo et al., 2011). Then, 8 g V/Fe/Mt was dispersed in 400 mL water again, which was mixed with $Bi(NO_3)_3$ solution (cooled to 60 °C) under magnetic stirring until the molar ratio of Bi/V reached 1. After stirring for 24 h, the product was centrifuged and washed. According to the amount of added $BiVO_4$, the resulting materials were denoted as 1%, 2%, 4%, 8%, 10%, and 15%$BiVO_4$/Fe/Mt, respectively.

For comparison purpose, the pure $BiVO_4$ was prepared by adding NH_4VO_3 solution into $Bi(NO_3)_3$ solution under constant magnetic stirring at 60 °C for 24 h. All of the obtained samples were washed with deionized water until the supernatant pH was close to neutral. After that, the products were freeze-dried under −40 °C, and pulverized to pass through a 200-mesh sieve.

2.3. Characterization

X-ray diffraction (XRD) patterns of the prepared samples were acquired with a Bruker D8 ADVANCE X-ray diffractometer. The measurements were operated at 40 kV and 40 mA with Cu Kα irradiation, and the 2θ range between 1° and 70° was recorded with a scanning speed of 2°/min in the humidity range of 42%–44%.

Nitrogen adsorption–desorption isotherms were measured on a Micromeritics ASAP 2020M instrument. Before the adsorption tests, the samples were outgassed for 12 h at 30 °C. The multiple-point Brunauer–Emmett–Teller (BET) method was used to calculate the specific surface areas of the samples.

The UV–vis diffuse reflectance spectra were measured by Shimadzu UV-2550 double-beam digital spectrophotometer equipped with conventional components of a reflectance spectrometer, and $BaSO_4$ was used as reference.

The chemical compositions of the samples were determined using Agilent 7700× inductively coupled plasma mass spectrometry (ICP-MS).

2.4. Photocatalytic tests and analytical methods

The photocatalytic activity of the obtained samples was determined by the degradation of AR18 under various conditions. The experiments were conducted in a photochemical reaction instrument (BL-GHX-V, Shanghai Depai Biotech. Co. Ltd., China). To simulate the visible spectrum, a 400 W halogen lamp (420–780 nm, 21.5–23.0 mw/cm^2) was applied as the light source with a cutoff filter to filter out the light with wavelengths below 420 nm, and the filter was positioned inside a cylindrical Pyrex vessel surrounded by a circulating water jacket.

In the photocatalytic activity evaluation experiments, 0.4 g/L of catalyst (except for pure $BiVO_4$, 4.2×10^{-2} g/L, the same amount of $BiVO_4$ on $BiVO_4$/Fe/Mt) was added to 50 mL AR18 (1.3×10^{-4} mol/L, pH 3) aqueous solution. The initial pH value of the solution was adjusted by adding NaOH or HNO_3. All experiments were carried out under constant stirring to ensure good dispersion of the catalysts. The reaction was started when the halogen lamp was turned on and H_2O_2 (0.8×10^{-2} mol/L) was added to AR18 solution. During the photolysis process, samples were collected at desired intervals from the solution, which was followed by centrifugation to separate the solid from the liquid before measurement.

The AR18 concentration was quantified by its absorbance at a wavelength of 509 nm with a spectrophotometer (759S, Shanghai JingHua Instrument Co. Ltd., China). The amount of Fe ions leached from catalysts into the solution was determined by atomic absorption spectrophotometry (PerkinElmer AAnalyst 400, America). Total organic carbon (TOC) was measured by a TOC analyzer (Shimadzu TOC-V CPH, Japan) equipped with an autosampler.

•OH generated in the heterogeneous photo-Fenton systems were trapped with DMSO to produce formaldehyde quantitatively, which then reacted with DNPH to form hydrazone (DNPHo) and were analyzed by high performance liquid chromatography (HPLC, Agilent 1200 LC), equipped with an Agilent Eclipse XDB-C18 column (150 mm × 4.6 mm, particle size 5 μm). The details of analysis procedure were described according to the paper of Zhong et al. (2014).

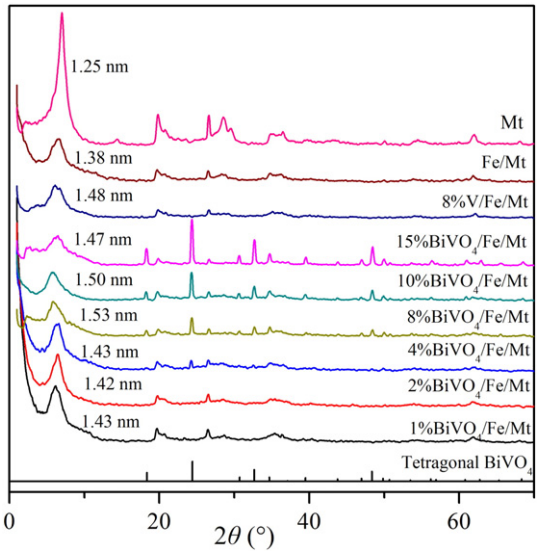

Fig. 1. The XRD patterns of samples.

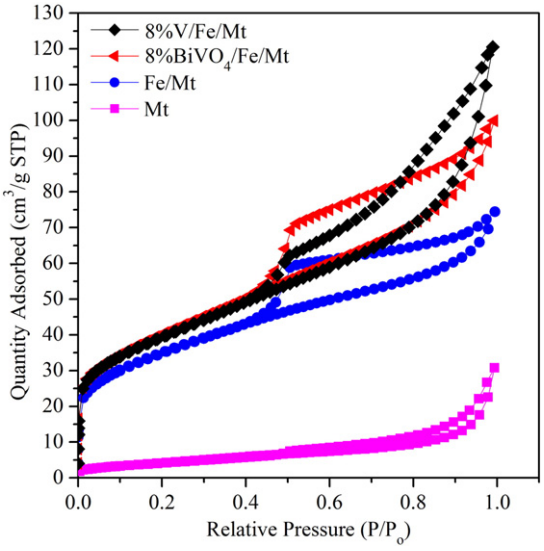

Fig. 2. Nitrogen adsorption–desorption isotherms of samples.

2.5. Photocatalytic stability experiments

8%$BiVO_4$/Fe/Mt was used repeatedly to degrade AR18 to evaluate its photocatalytic stability. The experimental process was similar to the above photocatalytic experiment. After reaction in each run, the photocatalyst was collected by centrifugation for the next use.

3. Results and discussion

3.1. Structural characterization results

XRD characterization is one of the most effective methods to study the basal spacing of clay minerals, which can be determined from the 001 reflection. The XRD patterns of the samples (Fig. 1) revealed that the basal spacing values of Mt and Fe/Mt were approximately 1.25 and 1.38 nm, respectively, indicating the intercalation of hydroxy-iron cations into the interlayers of Mt. The continuous increase of basal spacing after the addition of V and Bi (i.e., approximately 1.48 nm for 8%V/Fe/Mt and 1.53 nm for 8%$BiVO_4$/Fe/Mt) suggested the intercalation of V and Bi into the interlayers of Mt as well. In addition, the XRD pattern of $BiVO_4$/Fe/Mt showed characteristic reflections at 24°, 32°, and 48° (2θ) except for the low content of $BiVO_4$ (1% and 2%), which were in agreement with the standard data of tetragonal $BiVO_4$ (JCPD no: 14-0133).

The bulk Fe, Bi, and V concentrations of the samples with respect to their total weight were measured by ICP-MS (Table 1), which showed that the molar ratio of Bi/V was close to 1 on 8%$BiVO_4$/Fe/Mt, in agreement with the theoretical ratio of $BiVO_4$. Combining the XRD and ICP-MS results, one can tell that $BiVO_4$ existed both on the outer surface and within the interlayers of Mt.

The nitrogen adsorption–desorption isotherms of the obtained samples (Fig. 2) can be classified as type IV shape (Brunauer–Deming–Deaming–Teller) and type H3 hysteresis loop (International Union of Pure and Applied Chemistry classification) (Kruk and Jaroniec, 2001), suggesting the presence of mesopores with slit-shape on these samples (Gunjakar et al., 2011). In addition, Fe/Mt, 8%V/Fe/Mt, and $BiVO_4$/Fe/Mt showed significant adsorption of nitrogen at a low relative pressure range, suggesting the apparent presence of micropores on these samples as well. According to the calculated specific surface area (SSA) of the samples (Table 1 and Table S1), both 8%V/Fe/Mt and (1%, 2%, 4%, 8%, 10%, 15%) $BiVO_4$/Fe/Mt had better SSA and as compared with Fe/Mt.

The UV–vis diffused reflectance spectra of the samples (Fig. 3) showed that pure $BiVO_4$ had photoabsorption from UV light to visible light, and the wavelength of the absorption edge was 525 nm. After the loading of $BiVO_4$ on Fe/Mt, however, the absorption bands of 8%$BiVO_4$/Fe/Mt showed a slight blue shift as compared to that of Fe/Mt. In addition, the absorption bands of $BiVO_4$/Fe/Mt with varying $BiVO_4$ contents first increased with the increasing content of $BiVO_4$, and then begun to decrease when the content of $BiVO_4$ was larger than 4% (Fig. 1S). Whereas, $BiVO_4$/Fe/Mt had a significant absorption in the visible light region up to 600 nm, indicating that $BiVO_4$/Fe/Mt can be a potential photocatalyst as well for visible-light-driven applications.

Table 1
The structural characteristics of various samples.

Samples	SSA (m^2/g)	Total pore volume (cm^3/g)	Fe (mt%)	Bi (mt%)	V (mt%)
Mt	16.5	0.035	–	–	–
Fe/Mt	125.5	0.108	26.0	–	–
8%V/Fe/Mt	144.2	0.145	21.2	–	1.33
8%$BiVO_4$/Fe/Mt	141.0	0.170	20.2	5.62	1.26

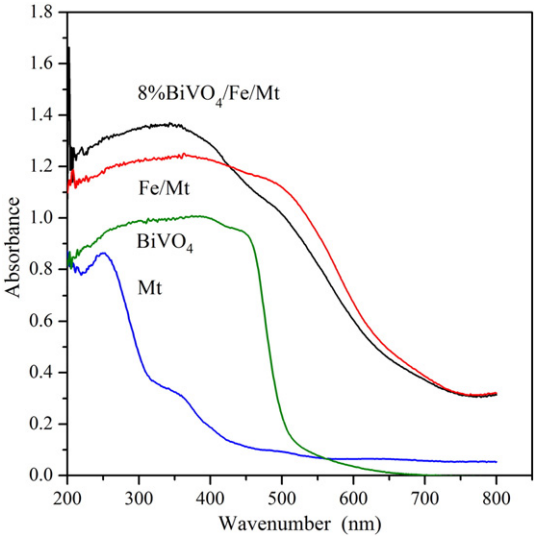

Fig. 3. UV–vis diffuse reflectance spectra of samples.

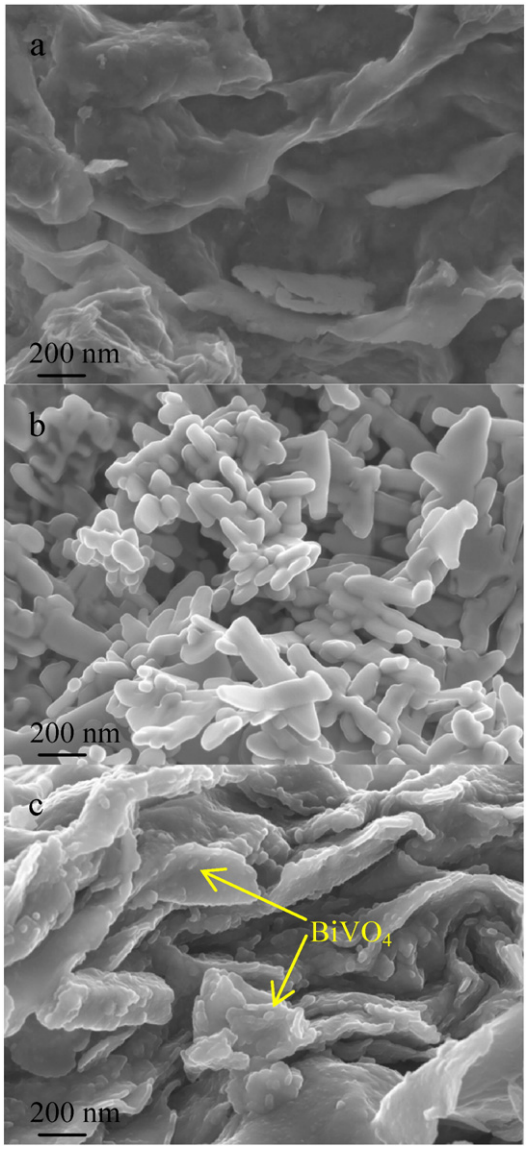

Fig. 4. SEM images of samples. a. Fe/Mt; b. $BiVO_4$; c: 8%$BiVO_4$/Fe/Mt.

Morphologies of the samples were characterized by SEM (Fig. 4a–c). As shown in Fig. 4a, the Fe/Mt displayed lamellar structures, and the pure $BiVO_4$ showed a large particle of irregular morphology (Fig. 4b). When Fe/Mt dispersion was introduced into the synthetic system, the diameter of $BiVO_4$ gradually decreased, which was much less than those of pure $BiVO_4$ (Fig. 4c). This phenomenon indicated an obvious tailoring effect of Fe/Mt relative to the size of the $BiVO_4$ particles on the composites. This was probably because negatively charged vanadate binded directly to the surface of positively charged Fe/Mt via electrostatic interaction. Then, Bi^{3+} combined to phosphate to form $BiVO_4$, which to some extent hindered the generation of the $BiVO_4$ seed particles and controlled the growth of the $BiVO_4$ particles.

3.2. Decolorization and mineralization of AR18

To investigate the photocatalytic activities of the as-prepared photocatalysts, several photocatalytic experiments using the samples with varying $BiVO_4$ content were carried out for AR18 degradation under visible light irradiation (Fig. 5a–c). The results showed that the decolorization efficiency (Fig. 5a) and TOC removal efficiency (Fig. 5b) of AR18 first increased with the increasing content of $BiVO_4$, and then begun to decrease when the content of $BiVO_4$ was larger than 8%. Moreover, the Fe leaching (Fig. 5c) from 8%$BiVO_4$/Fe/Mt after 180 min reaction was the lowest. Thus, the optimal photocatalyst was 8%$BiVO_4$/Fe/Mt, and its structural characteristics and photocatalytic reactivity were studied in detail in this article.

Decolorization efficiency and TOC removal efficiency of AR18 under various experimental conditions were examined to investigate the photocatalytic activities of 8%$BiVO_4$/Fe/Mt and Fe/Mt (Fig. 6). With only visible light (Fig. 6, curve i), the decolorization of AR18 was just about 8.0%, with negligible TOC removal efficiency, which indicated that AR18 can resist visible light. Both the '8%$BiVO_4$/Fe/Mt + visible light' system and the 'Fe/Mt + visible light' system showed insignificant decolorization and mineralization of AR18 (Fig. 6, curve g and h), which implied that both 8%$BiVO_4$/Fe/Mt and Fe/Mt had poor adsorption capacity of AR18. On the other hand, as the 'Fe/Mt + H_2O_2' system and the '8%$BiVO_4$/Fe/Mt + H_2O_2' system (Fig. 6, curve f and e) were composed of a Fenton-like reaction, the decolorization of AR18, therefore, could reach 37.1% and 56.4% respectively after 180 min reaction; however, both of the two systems showed low mineralization of AR18.

Significant decolorization of AR18 (79.2%) was observed in the 'H_2O_2 + visible light' system (Fig. 6, curve d), and it was further slightly increased after the addition of $BiVO_4$ (i.e., the '$BiVO_4$ + H_2O_2 + visible light' system) (Fig. 6, curve c). In both the two systems, nearly 10% TOC of AR18 was removed after 180 min reaction. These results indicated that $BiVO_4$ had a weak ability for the catalytic decolorization and mineralization of AR18 under the tested conditions.

As for the 'Fe/Mt + H_2O_2 + visible light' system (Fig. 6, curve b), the decolorization of AR18 was faster than those under control conditions (Fig. 6, curves d, h and i), but slower than that using 8%$BiVO_4$/Fe/Mt as a catalyst (Fig. 6, curve a), and the time needed to reach a steady state in the two systems were 80 and 40 min, respectively. Complete decolorization of AR18 in the two systems could be achieved after 180 min. Meanwhile, the TOC removal of AR18 in the 'Fe/Mt + H_2O_2 + visible

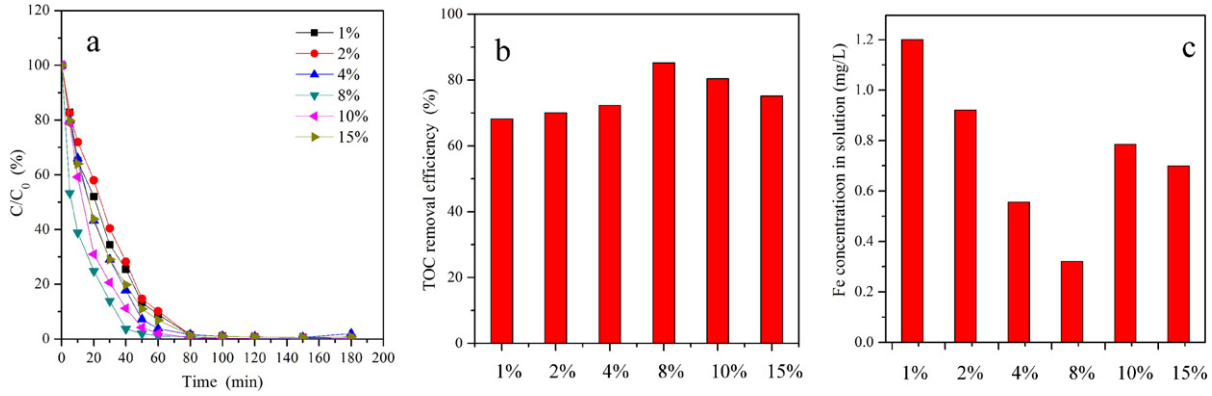

Fig. 5. The photocatalytic tests of $BiVO_4$/Fe/Mt with varying $BiVO_4$ content. a. Decolorization of acid red 18; b. mineralization of acid red 18; c. Fe concentration in solution.

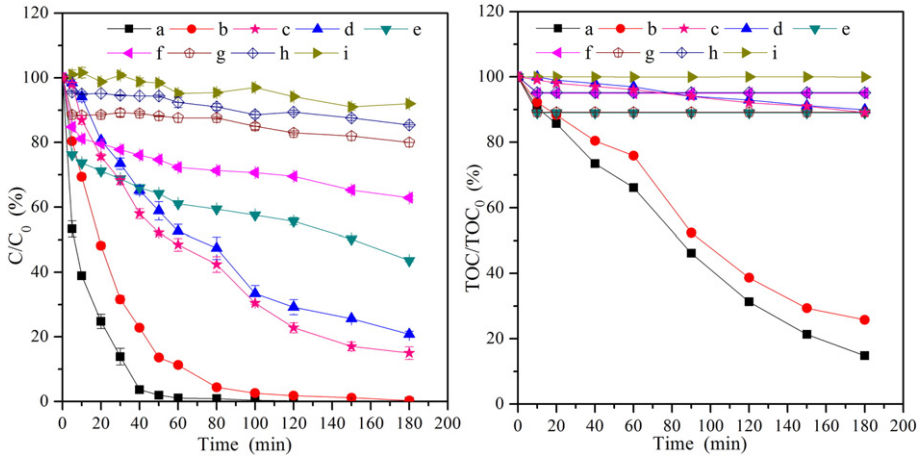

Fig. 6. Decolorization and mineralization of acid red 18 under different conditions. a. 8%$BiVO_4$/Fe/Mt + H_2O_2 + visible light; b. Fe/Mt + H_2O_2 + visible light; c. $BiVO_4$ + H_2O_2 + visible light; d. H_2O_2 + visible light; e. 8%$BiVO_4$/Fe/Mt + H_2O_2; f. Fe/Mt + H_2O_2; g. 8%$BiVO_4$/Fe/Mt + visible light; h. Fe/Mt + visible light; i. visible light.

light' system was increased with the reaction time, and the removal efficiency reached 74.2% after 180 min. However, great enhancement of the mineralization rate (85.2%) was observed when using 8%$BiVO_4$/Fe/Mt as the catalyst. These results showed that 8%$BiVO_4$/Fe/Mt had better catalytic activity than Fe/Mt and $BiVO_4$ for the degradation of AR18.

The decolorization kinetics of AR18 was fitted with the pseudo-first-order equation. The rate constant was obtained from the slope of a straight line by plotting the value of $\ln(C/C_0)$ against the reaction time (Fig. 7). According to the calculated values, the rate constants follow the order: '8%$BiVO_4$/Fe/Mt + H_2O_2 + visible light' system > 'Fe/Mt + H_2O_2 + visible light' system > 'H_2O_2 + visible light' system, which clearly showed that 8%$BiVO_4$/Fe/Mt had better catalytic activity than Fe/Mt.

3.3. •OH generation in the heterogeneous photo-Fenton systems

The high generation rate of •OH in the '8%$BiVO_4$/Fe/Mt + H_2O_2 + visible light' system and in the 'Fe/Mt + H_2O_2 + visible light' system was observed (Fig. 8). The concentration of •OH in the two systems increased with the reaction time, and then levelled off after 150 min reaction. In addition, the former system clearly generated a higher concentration of •OH than the later one (e.g., 1062.2 vs. 953.2 μmol/L after 180 min reaction). The remarkable •OH generation performance of 8%$BiVO_4$/Fe/Mt suggested that the presence of $BiVO_4$ could accelerate the generation of •OH.

3.4. Stability test of photocatalysts

In order to determine the stability of the catalysts, Fe concentration in the solutions after 180 min reaction in different systems was measured (Fig. 9). The results showed that visible light could lead to Fe leaching, which can be attributed to the photodissolution of 8%$BiVO_4$/Fe/Mt and Fe/Mt (Fig. 9, columns g and h) (Waite and Morel, 1984). Meanwhile, the presence of H_2O_2 also had an effect on Fe leaching from 8%$BiVO_4$/Fe/Mt and Fe/Mt (Fig. 9, columns e and f).

The insert in Fig. 9 showed the Fe leaching concentrations in the '8%$BiVO_4$/Fe/Mt + H_2O_2 + visible light' system and the 'Fe/Mt + H_2O_2 + visible light' system (Fig. 9, curves a and b) as a function of reaction time. Apparently, the Fe leaching concentration in the '8%$BiVO_4$/Fe/Mt + H_2O_2 + visible light' system (Fig. 9, curve a) was lower than that in the 'Fe/Mt + H_2O_2 + visible light' system (Fig. 9, curve b) in the whole process, but both the two systems had a similar Fe leaching behavior. In particular, Fe leaching in both systems first increased with reaction time, and then begun to decrease after 120 min reaction. After 180 min reaction, the Fe concentration in the solution was only 0.32 mg/L (or 0.4%) for the '8%$BiVO_4$/Fe/Mt + H_2O_2 + visible light' system and 0.66 mg/L (or 0.7%) for the 'Fe/Mt + H_2O_2 + visible light'

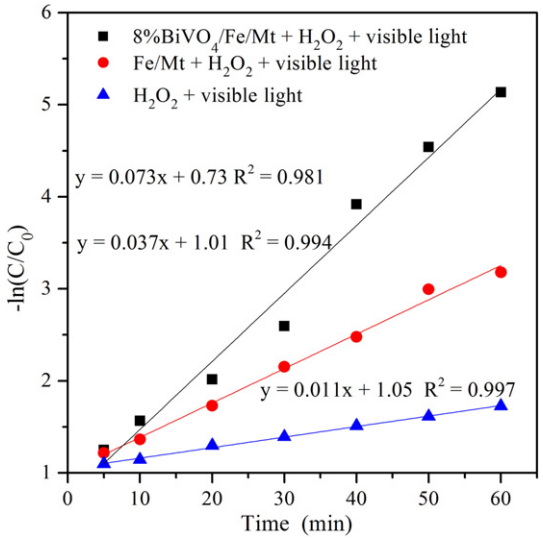

Fig. 7. The decolorization kinetics of acid red 18 at different conditions.

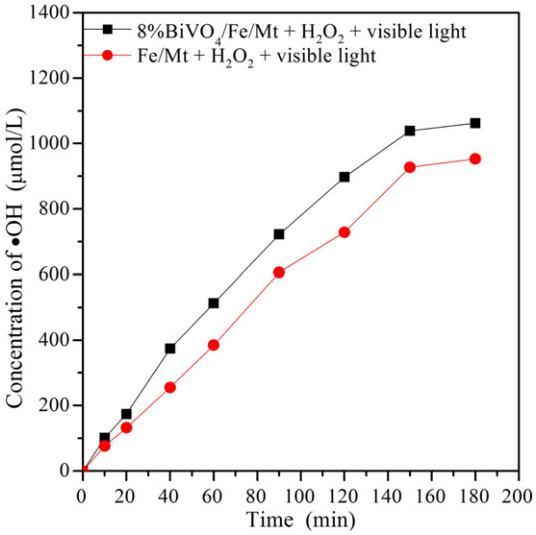

Fig. 8. The concentration of •OH in the heterogeneous photo-Fenton systems.

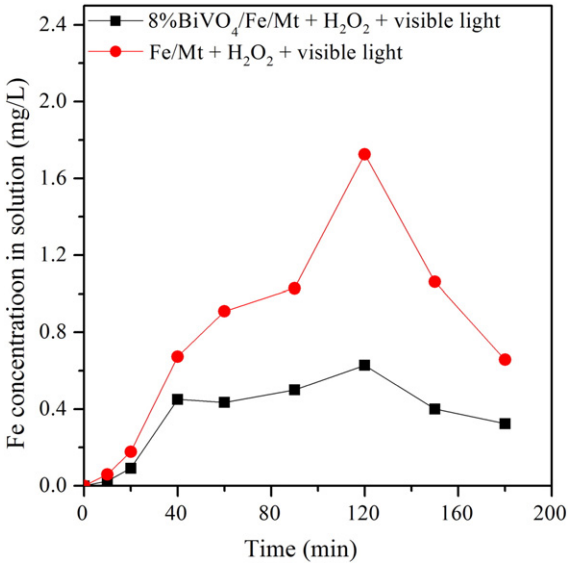

Fig. 9. Fe concentration in solution as a function of time.

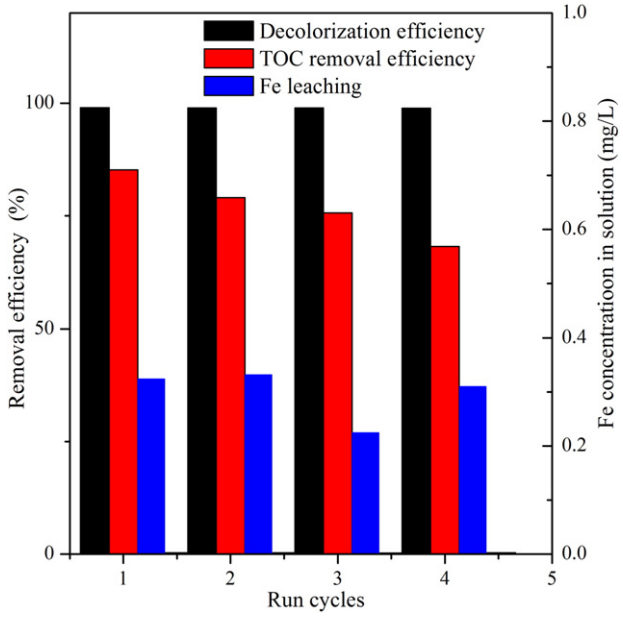

Fig. 10. Stability test of 8%$BiVO_4$/Fe/Mt.

system. These results suggested that 8%$BiVO_4$/Fe/Mt was more stable than Fe/Mt in the heterogeneous photo-Fenton reaction process.

Furthermore, the long-term stability of a catalyst is a key issue for its practicality. The results of the stability test of 8%$BiVO_4$/Fe/Mt (Fig. 10) showed that the decolorization efficiency of AR18 (>98%) was still efficient after being used for 4 cycles, though the TOC removal efficiency of AR18 was slightly decreased. The Fe concentration in the solution was still lower than 0.4 mg/L after repeating the reaction for 4 cycles, implying that 8%$BiVO_4$/Fe/Mt was very stable. Meanwhile, those values were also higher than the degradation efficiency of reactive brilliant orange (93%) over iron-pillared Mt and TOC removal of azocarmine B (about 38%) over the hydroxyl iron–aluminum pillared bentonite after three times recycling reported in the reference (Chen et al., 2009; Xu et al., 2014).

3.5. Comparison of heterogeneous and homogeneous photo-Fenton processes

In order to evaluate the contribution from the homogeneous photo-Fenton process for the decolorization and mineralization of AR18 by 8%$BiVO_4$/Fe/Mt, the highest and the final concentrations of total Fe ions leached from the 8%$BiVO_4$/Fe/Mt (0.63 mg/L and 0.32 mg/L, Fig. 9, curve a) were chosen as the initial Fe^{3+} concentration in the homogeneous photo-Fenton process. The results showed that the decolorization of AR18 were all over 98% after 180 min reaction for all the three systems (Fig. 11). However, the mineralization rate of AR18 in the heterogeneous photo-Fenton was much faster than those in the homogeneous photo-Fenton processes. After 180 min reaction, the TOC removal values of 85.2%, 40.3%, and 21.9% were obtained in the '8%$BiVO_4$/Fe/Mt + H_2O_2 + visible light' system, '0.63 mg/L Fe^{3+} + H_2O_2 + visible light' system, and '0.32 mg/L Fe^{3+} + H_2O_2 + visible light' system, respectively. Hence, the contribution of the heterogeneous photo-Fenton reaction was quite significant for the mineralization of AR18.

3.6. Possible mechanism for the enhanced photocatalytic activity

The above results, showed that in the heterogeneous photo-Fenton process $BiVO_4$/Fe/Mt had better performance in the degradation of AR18 and •OH generation than Fe/Mt, but the Fe leaching from the latter was more serious than that from the former, which proved the synergistic effect between Fe and $BiVO_4$ on $BiVO_4$/Fe/Mt in the degradation of AR18. The possible contributions for the enhanced photocatalytic activity of $BiVO_4$/Fe/Mt may originate from two aspects (Fig. 12).

One was from the oxidation of AR18 by free radicals produced by $BiVO_4$. As $BiVO_4$ is an n-type oxide semiconductor, visible light irradia-

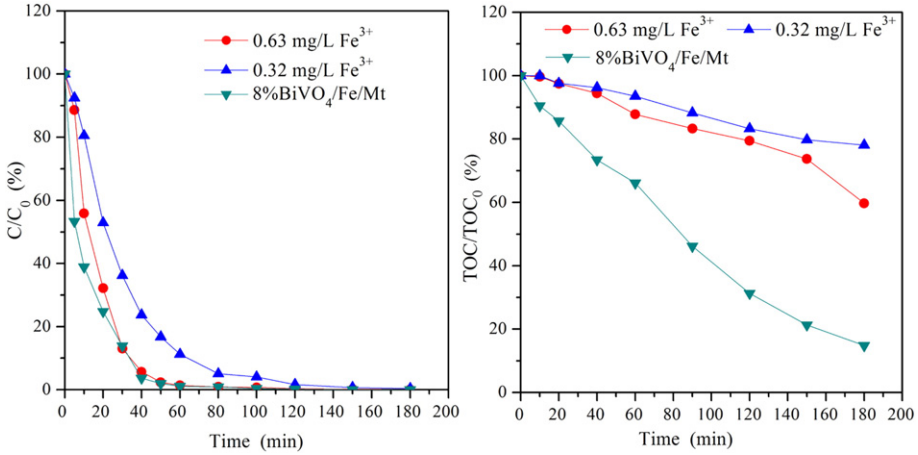

Fig. 11. Decolorization and mineralization of acid red 18 in the heterogeneous and corresponding homogeneous photo-Fenton systems.

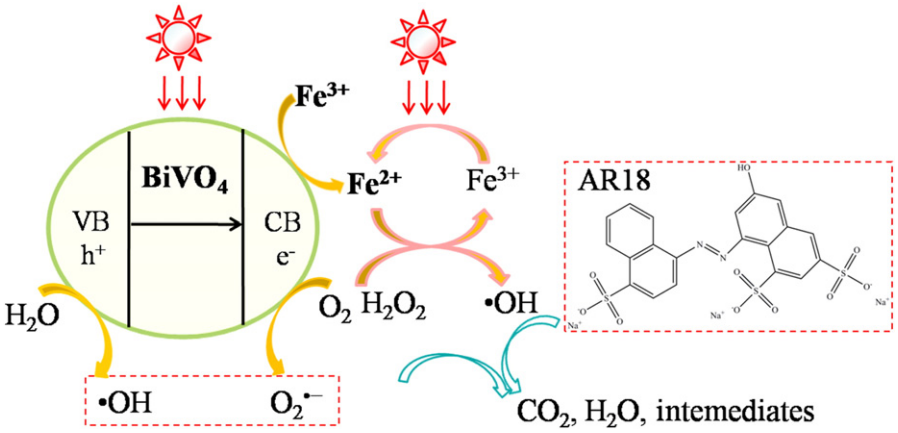

Fig. 12. Possible photocatalytic mechanism.

tion leads to the promotion of electrons (e^-) from the valence band (VB) to the conduction band (CB), leaving holes (h^+) in the VB (Long et al., 2006). The e^- in CB may react with O_2 in the solution producing $O_2^{\bullet -}$, and the h^+ in VB may react with H_2O producing •OH.

Another was from the oxidation of AR18 by •OH originating from the heterogeneous photo-Fenton reaction. Ge et al. (2012) observed that in the $BiVO_4/Fe^{3+}$ system Fe^{3+} was reduced to Fe^{2+} by photo-induced electrons, which could prevent the electron–hole recombination and then enhance the degradation of RhB. Sasaki et al. (2008) also reported that Fe^{3+} can act as an electron acceptor in the ($Ru/SrTiO_3$:Rh)-($BiVO_4$) photocatalysis system for water splitting. Therefore, in this work we propose that the Fe^{3+} on $BiVO_4$/Fe/Mt could accept the photoinduced electrons from $BiVO_4$ and be reduced to Fe^{2+}. This reduction can prevent the electron–hole recombination, and then help in enhancing the catalytic activity of $BiVO_4$ as well. In addition, with the accelerated reduction of Fe^{3+} into Fe^{2+} under visible light irradiation, the decomposition of H_2O_2 into highly oxidative •OH can be accelerated.

4. Conclusion

A $BiVO_4$/Fe/Mt composite was synthesized successfully by using Fe/Mt as a host material to load $BiVO_4$. The combination of XRD and ICP-MS results showed that $BiVO_4$ loaded not only on the outer surface but also into the interlays of Fe/Mt. Compared with Fe/Mt, 8%$BiVO_4$/Fe/Mt exhibited higher photocatalytic activity, and nearly complete decolorization was achieved while 85.2% TOC removal was attained under proper conditions; meanwhile, the Fe leaching was 0.32 mg/L and the concentrations of •OH was 1062.2 μmol/L after 180 min reaction. The high AR18 decolorization efficiency and TOC removal efficiency, low Fe leaching and remarkable •OH generation performance by 8%$BiVO_4$/Fe/Mt was probably because $BiVO_4$ and Fe had a synergistic effect. More specifically, the Fe^{3+} on $BiVO_4$/Fe/Mt could accept the photoinduced electrons from $BiVO_4$ and be reduced to Fe^{2+}, which subsequently could prevent the electron–hole recombination and accelerate reduction of Fe^{3+} into Fe^{2+}. As a result, the production of highly oxidative •OH can be enhanced as well.

Acknowledgements

This work was financially supported by the National Natural Science Foundation of China (41572031,41322014, 21177104), "One Hundred Talents Program" of CAS (KZZD-EW-TZ-10), the National Youth Top-notch Talent Support Program Newton Advanced Fellowship (NA150190), the Guangdong Provincial Youth Top-notch Talent Support Program (2014TQ01Z249), the CAS/SAFEA International Partnership Program for Creative Research Teams (20140491534), and the Research Foundation of Education Bureau of Hunan Province, China (No. 14B177).This is a contribution (No.IS-2228) from GIGCAS.

Appendix A. Supplementary data

Supplementary data to this article can be found online at http://dx.doi.org/10.1016/j.clay.2016.04.018.

References

Ai, N.S., Hameed, B.H., 2011. Heterogeneous catalytic treatment of synthetic dyes in aqueous media using Fenton and photo-assisted Fenton process. Desalination 269, 1–16.
Carriazo, J., Guelou, E., Barrault, J., Tatibouet, J., Moreno, S., 2003. Catalytic wet peroxide oxidation of phenol over Al–Cu or Al–Fe modified clays. Appl. Clay Sci. 22, 303–308.
Chen, J., Zhu, L., 2007. Heterogeneous UV-Fenton catalytic degradation of dyestuff in water with hydroxyl-Fe pillared bentonite. Catal. Today 126, 463–470.
Chen, Q., Wu, P., Li, Y., Zhu, N., Dang, Z., 2009. Heterogeneous photo-Fenton photodegradation of reactive brilliant orange X-GN over iron-pillared montmorillonite under visible irradiation. J. Hazard. Mater. 168, 901–908.
Daud, N., Ahmad, M., Hameed, B., 2010. Decolorization of acid red 1 dye solution by Fenton-like process using Fe–montmorillonite K10 catalyst. Chem. Eng. J. 165, 111–116.
De León, M.A., Sergio, M., Bussi, J., 2013. Iron-pillared clays as catalysts for dye removal by the heterogeneous photo-Fenton technique. React. Kinet. Mech. Catal. 110, 101–117.
Epstein, M., Yariv, S., 2003. Visible-spectroscopy study of the adsorption of alizarinate by Al–montmorillonite in aqueous suspensions and in solid state. J. Colloid Interface Sci. 263, 377–385.
Feng, J., Hu, X., Yue, P.L., Zhu, H.Y., Lu, G.Q., 2003. Discoloration and mineralization of reactive red HE-3B by heterogeneous photo-Fenton reaction. Water Res. 37, 3776–3784.
Feng, J., Hu, X., Yue, P.L., 2004. Discoloration and mineralization of Orange II using different heterogeneous catalysts containing Fe: a comparative study. Environ. Sci. Technol. 38, 5773–5778.
Garrido-Ramírez, E., Theng, B., Mora, M., 2010. Clays and oxide minerals as catalysts and nanocatalysts in Fenton-like reactions—a review. Appl. Clay Sci. 47, 182–192.
Ge, M., Liu, L., Chen, W., Zhou, Z., 2012. Sunlight-driven degradation of rhodamine B by peanut-shaped porous $BiVO_4$ nanostructures in the H_2O_2-containing system. CrystEngComm 14, 1038–1044.
Gunjakar, J.L., Kim, T.W., Kim, H.N., Kim, I.Y., Hwang, S.-J., 2011. Mesoporous layer-by-layer ordered nanohybrids of layered double hydroxide and layered metal oxide: highly active visible light photocatalysts with improved chemical stability. J. Am. Chem. Soc. 133, 14998–15007.
Guo, Z., Li, Y., Zhang, S., Niu, H., Chen, Z., Xu, J., 2011. Enhanced sorption of radiocobalt from water by Bi (III) modified montmorillonite: a novel adsorbent. J. Hazard. Mater. 192, 168–175.
Herney-Ramirez, J., Vicente, M.A., Madeira, L.M., 2010. Heterogeneous photo-Fenton oxidation with pillared clay-based catalysts for wastewater treatment: a review. Appl. Catal. B Environ. 98, 10–26.
Karamanis, D., Assimakopoulos, P.A., 2007. Efficiency of aluminum-pillared montmorillonite on the removal of cesium and copper from aqueous solutions. Water Res. 41, 1897–1906.
Kavitha, P., Shavonda, M., Changseok, H., Miguel, P., Xiaojia, H., Dionysiou, D.D., Huey-Min, H., 2013. Photo-inactivation of *Escherichia coli* by sulfur and nitrogen-fluorine-codoped TiO_2 nanoparticles under solar simulated light and visible light irradiation. Environ. Sci. Technol. 47, 9988–9996.
Konstantinou, I.K., Albanis, T.A., Petrakis, D.E., Pomonis, P.J., 2000. Removal of herbicides from aqueous solutions by adsorption on Al-pillared clays, Fe–Al pillared clays and mesoporous alumina aluminum phosphates. Water Res. 34, 3123–3136.
Kruk, M., Jaroniec, M., 2001. Gas adsorption characterization of ordered organic–inorganic nanocomposite materials. Chem. Mater. 13, 3169–3183.
Long, M., Cai, W., Cai, J., Zhou, B., Chai, X., Wu, Y., 2006. Efficient photocatalytic degradation of phenol over $Co_3O_4/BiVO_4$ composite under visible light irradiation. J. Phys. Chem. B 110, 20211–20216.

Ramesh, A., Hasegawa, H., Maki, T., Ueda, K., 2007. Adsorption of inorganic and organic arsenic from aqueous solutions by polymeric Al/Fe modified montmorillonite. Sep. Purif. Technol. 56, 90–100.

Sasaki, Y., Iwase, A., Kato, H., Kudo, A., 2008. The effect of co-catalyst for Z-scheme photocatalysis systems with an Fe^{3+}/Fe^{2+} electron mediator on overall water splitting under visible light irradiation. J. Catal. 259, 133–137.

Waite, T.D., Morel, F.M., 1984. Photoreductive dissolution of colloidal iron oxides in natural waters. Environ. Sci. Technol. 18, 860–868.

Wang, Z., Yin, L., Chen, Z., Zhou, G., Shi, H., 2014. Photodegradation of methyl Orange using magnetically recoverable $AgBr@Ag_3PO_4/Fe_3O_4$ photocatalyst under visible light. J. Nanomater. 2, 87–95.

Wang, Y., Su, X., Lin, X., Zhang, P., Wen, K., Zhu, J., He, H., 2015. The non-micellar template model for porous clay heterostructures: a perspective from the layer charge of base clay. Appl. Clay Sci. 116, 102–110.

Wu, P., Wu, W., Li, S., Xing, N., Zhu, N., Li, P., Wu, J., Yang, C., Dang, Z., 2009. Removal of Cd^{2+} from aqueous solution by adsorption using Fe-montmorillonite. J. Hazard. Mater. 169, 824–830.

Xi, G., Yue, B., Cao, J., Ye, J., 2011. Fe_3O_4/WO_3 hierarchical core–shell structure: high-performance and recyclable visible-light photocatalysis. Chem. Eur. J. 17, 5145–5154.

Xu, T., Liu, Y., Ge, F., Ouyang, Y., 2014. Simulated solar light photooxidation of azocarmine B over hydroxyl iron–aluminum pillared bentonite using hydrogen peroxide. Appl. Clay Sci. 100, 35–42.

Zhong, Y., Liang, X., He, Z., Tan, W., Zhu, J., Yuan, P., Zhu, R., He, H., 2014. The constraints of transition metal substitutions (Ti, Cr, Mn, Co and Ni) in magnetite on its catalytic activity in heterogeneous Fenton and UV/Fenton reaction: from the perspective of hydroxyl radical generation. Appl. Catal. B Environ. 150-151, 612–618.